MAVEN Survey of Magnetic Flux Rope Properties in the Martian Ionosphere: Comparison with 3 Types of Formation Mechanisms

C. F. Bowers[1], J. A. Slavin[1], G. A. DiBraccio[2], G. Poh[2,3], T. Hara[4], S. Xu[4], D.A. Brain[5]

[1] Department of Climate and Space Sciences and Engineering, University of Michigan, Ann Arbor, Michigan, United States.

[2] Solar System Exploration Division, NASA Goddard Space Flight Center, Greenbelt, Maryland, USA.

[3] Center for Research and Exploration in Space Sciences and Technology II, Catholic University of America, Washington, D.C, USA.

[4] Space Sciences Laboratory, University of California, Berkeley, Berkeley, CA, USA.

[5] Laboratory for Atmospheric and Space Physics, University of Colorado, Boulder, CO, USA.

Key Points:

- Flux ropes form at Mars via three distinct processes: boundary wave instabilities, external reconnection, and internal reconnection.
- Across 1900 orbits, we identify and analyze 121 magnetic flux ropes within the ionosphere of Mars using observations from MAVEN.
- Using electron and magnetic field observations, we separate the flux ropes into three categories based on formation mechanism.

This is the author manuscript accepted for publication and has undergone full peer review but has not been through the copyediting, typesetting, pagination and proofreading process, which may lead to differences between this version and the Version of Record. Please cite this article as doi: 10.1029/2021GL093296.

Abstract

Flux ropes are a magnetic field phenomenon characterized by a filament of twisted, helical magnetic field around an axial core. They form in the Martian ionosphere via three distinct mechanisms: boundary wave instabilities (BWI), external reconnection (ER) between the interplanetary magnetic field and the crustal anomalies, and internal reconnection (IR) of the crustal anomalies themselves. We have identified 121 magnetic flux ropes from 1900 orbits using plasma and magnetic field measurements measured by the Mars Atmosphere and Volatile EvolutioN (MAVEN) spacecraft, and separate flux ropes into categories based on formation mechanism by analyzing electron signatures. We find evidence for flux ropes formed via BWI, ER, and IR mechanisms which comprise 9%, 34%, and 57% of our dataset, respectively. Flux ropes formed via different mechanisms exhibit differences in location and force-free radius, indicating the formation mechanism of a flux rope impacts their influence on the Martian plasma environment.

Plain Language Summary

Mars possess localized magnetic fields that are frozen into the crust of the planet and protrude out into space. On the dayside of Mars, the crustal fields interact with the charged particles and magnetic field lines that are emanating away from the Sun known as the solar wind. The processes involved in this interaction create the Martian "magnetosphere," and can have a variety of implications on the evolution of the Martian atmosphere. One by-product of this interaction is a "magnetic flux rope," which is a twisted filament of magnetic flux and plasma. Flux ropes show evidence for the reconfiguration of magnetic field lines within the magnetosphere, and lead to atmospheric loss at Mars. Using data from the Mars Atmosphere and Volatile EvolutioN (MAVEN) spacecraft, we analyze 121 events in which the spacecraft encountered a flux rope along its orbit around Mars. This is the first study to show evidence for Martian flux ropes having been formed via three distinct formation mechanisms. Flux ropes formed via different mechanisms exhibit differences in geographic location and size, indicating the formation mechanism of a flux rope impacts their influence on the Martian magnetospheric and atmospheric environment.

1 Introduction

Magnetic flux ropes (FR) are a well-documented space plasma physics phenomenon that have been detected throughout the solar system, ranging from the lower solar corona (*Fillipov et al.,*

2015) to the magnetosphere of Saturn (*Jasinski et al.*, 2016). An understanding of FRs and their formation is important for research in all space plasma environments for two main reasons: 1) FR formation plays a fundamental role in the reconfiguration of magnetic topology and 2) FRs have physical effects on the ambient environment, which includes storing magnetic energy and acting as channels for charged-particle transport. The ubiquity of FRs throughout diverse plasma environments suggests various processes are responsible for their formation.

At intrinsic magnetospheres, such as Earth and Mercury, planetary FRs are frequently observed along the dayside magnetopause and believed to form via multiple X-line reconnection between the interplanetary magnetic field (IMF) and the global intrinsic planetary magnetic field (e.g., *Lee and Fu,* 1985, *Sun et al.,* 2016). Multiple X-line reconnection also occurs to form FRs in the cross-tail current sheet where magnetic fields are oppositely oriented in the two lobes (e.g., *Elphic et al.,* 1986, *Slavin et al.,* 2003, *DiBraccio et al.,* 2015). On the dayside of planets with intrinsic magnetic fields, a high shear between the dipole magnetic field and the IMF along the magnetopause may result in single X-line reconnection or multiple X-line reconnection, the latter forming at least two magnetic FRs. After their formation on the dayside of the planet, these FRs subsequently carry magnetic flux and plasma to the nightside.

FRs have also been observed at Venus, Mars, and Titan where global intrinsic planetary magnetic fields are absent (e.g., *Wolff et al.,* 1980, *Luhmann et al.,* 1985, *Cloutier et al.*, 1999, *Penz et al.,* 2004, *Martin et al.,* 2020). These FRs must form through different processes than those observed at planets with a global, intrinsic magnetic dipole. At Venus, the IMF flux tubes penetrate into ionosphere and drape around the planet, and the barrier between the fast moving tailward flows of the magnetosheath and the slower moving ionospheric plasma (i.e., the ionopause) is subject to the development of large amplitude boundary wave instabilities. Simulation results have suggested that boundary wave instabilities such as Kelvin-Helmholtz (KH) may become non-linear and lead to FR formation at the ionopause of Venus (e.g., *Terada et al.*, 2002, *Möstl et al.,* 2011). These FRs were observed to be small-scale structures (~10 km in radius) and are evidence for the twisting of draped IMF flux tubes at the ionopause of Venus (*Luhmann et al.*, 1985).

FRs in the Martian induced magnetosphere are of particular interest due to the localized magnetic anomalies preserved by the crust of the planet (*Acuña., et al.,* 1999). In the southern hemisphere, the crustal anomalies are strong (~100-1000 nT at the surface) and protrude into space creating "mini-magnetospheres" similar to the IMF-planetary interactions along the dayside magnetopause of magnetized planets. In the northern hemisphere, the crustal anomalies

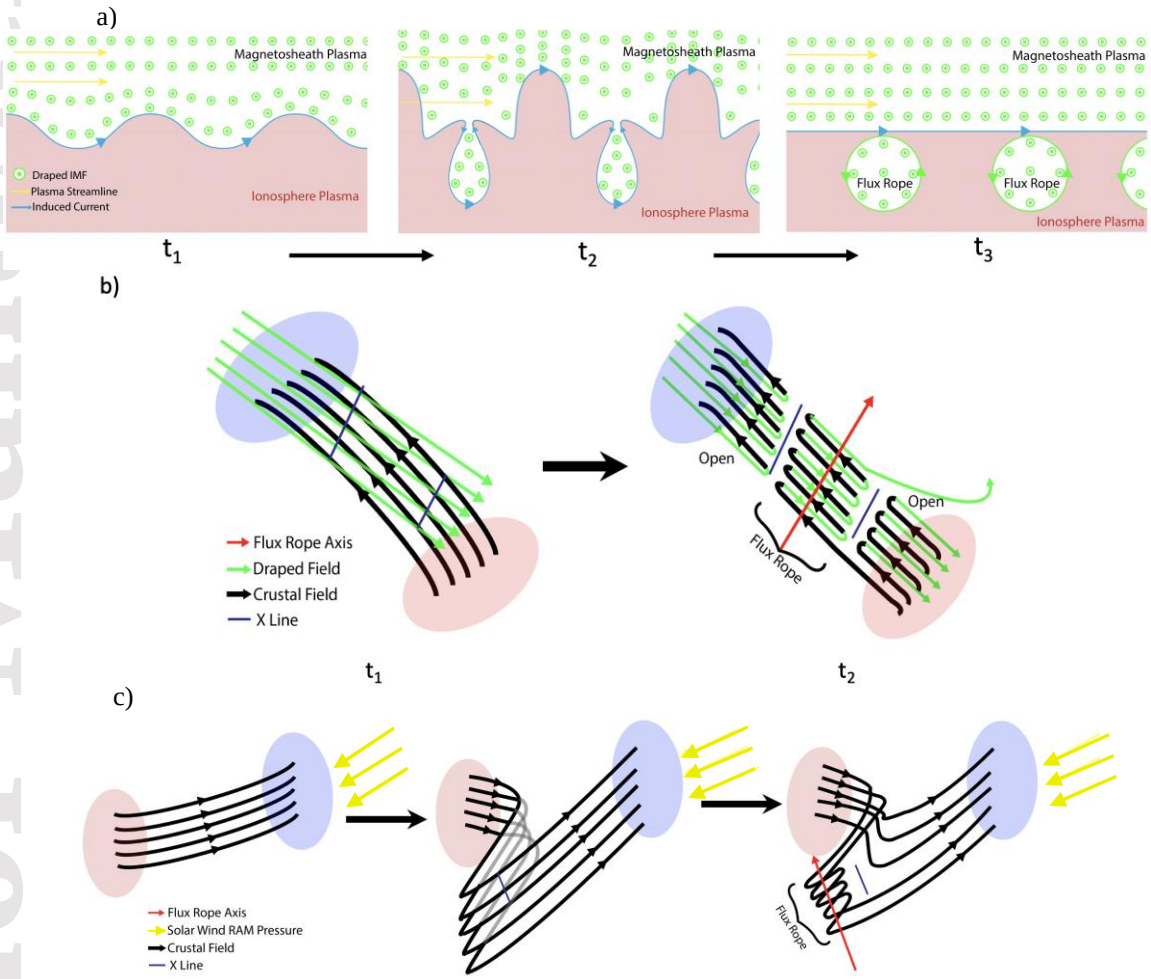

Figure **1**: *Schematic demonstrating how a flux rope may form under the (a) BWI mechanism, (b) ER mechanism, and (c) IR mechanism. Red and blue ovals represent regions of crustal fields that point radially outward and inward, respectively. Red arrows represent the right-handed flux rope axis. Arrows represent crustal magnetic field lines (black), draped IMF field lines (green), flowing sheath plasma streamlines (yellow), induced current (light blue), X-lines (dark blue).*

are much weaker, and do not inhibit the IMF flux tubes from penetrating deep into the ionosphere, creating a plasma environment similar to that at Venus. Together, these two

hemispheres comprise a unique hybrid magnetosphere at Mars. FRs play two major roles at Mars: 1) the rapid reconfiguration of planetary crustal magnetic fields and the acceleration of charged particles, and 2) atmospheric mass loss as planetary particles travel through their helical wraps and escape down the magnetotail (e.g., *Brain et al.,* 2010; *Hara et al.,* 2014; *Hara et al.,* 2017) .

Magnetic FRs have been observed in the Martian ionosphere by the Mars Global Surveyor (MGS) (e.g., *Cloutier et al.*, 1999; *Vignes et al.*, 2004; *Briggs et al.*, 2011; *Morgan et al.,* 2011; *Soobiah et al.,* 2014; *Hara et al.*, 2014) and the Mars Atmosphere and Volatile EvolutioN (MAVEN) spacecrafts (e.g., *Hara et al.,* 2017). The hybrid nature of Mars' magnetosphere suggests that these FRs may be created in processes similar to Venusian FRs formed by ionopause instabilities, or perhaps by a process unique to the Martian plasma environment. *Brain et al.,* [2010] first reported the MGS observation of an FR forming as a result of crustal field detachment due to magnetic reconnection. Using the plasma analysis capabilities of MAVEN, *Hara et al.,* [2017] also provided a detailed analysis of a similar event and demonstrated that this single ionospheric FR contained multiple planetary ions including H^+, O^+, O_2^+, and likely CO_2^+.

There is evidence that FRs at Mars may form via at least of the following three distinct mechanisms:

1. The development of boundary wave instabilities (BWI), most probably KH, on the boundary between the fast tailward flows in the magnetosheath and the slowly moving ionospheric plasma. KH waves have been detected at Mars (*Ruhunusiri et al.,* 2016), and if these boundary waves steepen sufficiently, the IMF flux tubes frozen into the magnetosheath plasma may become trapped and twisted (*Wolff et al.,* 1980; *Russell et al.,* 1990; *Wei et al.,* 2012), leading to FR formation as illustrated in Figure **1a**.
2. Multiple X-line external reconnection (ER) between the draped IMF and a crustal anomaly can form FRs in a manner similar to FR formation on the dayside magnetopause of intrinsically magnetized planets (*Hara et al.,* 2014, *Soobiah et al.,* 2014; *Hara et al.,* 2017), illustrated in Figure **1b**.
3. Single X-line internal reconnection (IR) of the crustal anomalies themselves (e.g., *Brain et al.,* 2010, *Morgan* et al., 2011; *Beharrell et al.,* 2012, *Hara et al.,* 2014). As the solar wind plasma flows around Mars, the ram pressure may stretch-out the crustal anomalies

as they respond to maintain pressure balance, leading to single X-line reconnection between the field lines of the anomalies resulting in FR formation illustrated in Figure **1c**.

Observations of FRs in the Martian ionosphere provide direct evidence for boundary wave instabilities or crustal field magnetic reconnection; however, there has been no comprehensive study of ionospheric FRs using the measurement capabilities of MAVEN to investigate their formation mechanisms. The work presented here conducts an extensive survey of FRs in the ionosphere of Mars. We use plasma data measured by MAVEN to estimate the magnetic topology of the FRs, providing evidence for three distinct formation mechanisms at Mars. Further analysis of the constituents, density, and velocity of the plasma contained within the FRs increases our understanding of their role in the fascinating topic of atmospheric mass loss at Mars.

2 Materials and Methods

2.1 Instrumentation

We investigate Martian FRs and their impact on the global magnetosphere and ionosphere through an analysis of data provided by the MAVEN spacecraft (*Jakosky et al.,* 2015). MAVEN's orbit precesses in both local time and longitude to provide global coverage of the Mars atmosphere and space environment with periapsis at ~150 km and apoapsis reaching ~6200 km. In particular, we analyze data provided by the Magnetometer (MAG) instrument (*Connerney et al.,* 2015) which measures vector magnetic fields at a maximum sampling rate of 32 vectors/s, the Solar Wind Electron Analyzer (SWEA) (*Mitchell et al.,* 2016), and the SupraThermal And Thermal Ion Composition (STATIC) instrument (*McFadden et al.,* 2015).

2.2 Methodology

Here, MAG data are analyzed in the Mars Solar Orbital (MSO) and Minimum Variance Analysis (MVA) coordinate system. The MSO coordinate system is defined so that the X-axis points from the center of Mars towards the Sun, the Z-axis points towards geographic north, and the Y-axis completes the right-handed coordinate system. Magnetic FR signatures identified in the MAG data depend heavily on the orientation of the FR, as well as the spacecraft trajectory through the structure. In order to account for this variability, we transform the magnetic field data into MVA coordinates (*Sonnerup and Scheible,* 1998). In the MVA coordinate system for an FR, the N-

direction defines the axis along which the magnetic field varies the least (i.e., minimum variance axis), and the N component (B_N) of the magnetic field remains steady throughout the extent of an FR. Note, the mean value of the B_N component of the magnetic field is smallest for spacecraft trajectories that pass closest to the center of quasi-cylindrical FRs. The M-direction (intermediate variance) points orthogonal to the N-direction and along the central axis of quasi-force free FRs (*Slavin et al.,* 2003). B_M for an FR would therefore exhibit a unimodal peak corresponding to the axial field enhancement at the center of the FR. The L-direction (maximum variance) completes the right-handed coordinate system and points in the direction of the bipolar magnetic field (B_L) signature defined by the outer helical wraps. The full amplitude of this bi-polar B_L signature maximizes for spacecraft trajectories passing closest to the central axis of the FR.

We also analyze superthermal (>1eV) electron data from the SWEA instrument onboard MAVEN to estimate the source of the electrons that populate the FR. SWEA is capable of measuring electron fluxes at a 4 second cadence. We use these fluxes compared to the local magnetic field orientation and spacecraft location to parameterize the electron distribution as demonstrated by *Weber et al.,* 2017. This parameter is known as the pitch angle distribution (PAD) score and is defined by: $(f_{FA}- f_{perp})/\sigma$, where f_{FA} is the electron flux in the field aligned direction (the most field-aligned 10° available within pitch angles 0-30° and 150-180°), f_{perp} is the electron flux in perpendicular direction (pitch angles 85-95°), and σ is the propagated uncertainty. PAD score distinguishes among 3 electron distributions: (1) field-aligned beam distribution (PAD score >2), (2) isotropic distribution (- 3< PAD score <2), (3) loss cone distribution (PAD score <-3). We also compare the electron energy distribution to an expected distribution for photoelectrons at Mars to parameterize the likelihood that the measured electrons are composed of primarily photoelectrons or solar wind electrons (*Xu et al.,* 2017); this is known as the shape parameter. The shape parameter distinguishes between two electron populations: 1) photoelectrons (shape parameter < 1) and 2) solar wind electrons (shape parameter > 1). Both the PAD score and shape parameter are calculated for populations that are moving towards Mars and away from Mars by measuring the local inclination of the magnetic field and comparing it with the pitch angle distribution of the electrons. *Xu et al.,* [2019] describes how to combine these parameters to estimate up to 7 types of topologies.

MAVEN has a precessing elliptical orbit where the spacecraft samples throughout the magnetosphere and into the solar wind. This ensures that there are extended periods in which the

spacecraft does not sample the low-altitude dayside of Mars, where we assume most of the ionospheric FRs form. From MAVEN observations taken between January 2015 and January 2019, we selected for orbits that sampled the low altitude (<1200 km) near-dayside (solar zenith angle (SZA) <110°) of the planet and visually inspected the MAG data for FR signatures.

3 Results

Throughout the 1900 orbits inspected, we identified 171 magnetic FRs. Of the 171 FRs identified, 156 show a sufficiently large (>2) max/intermediate eigenvalue ratio calculated from MVA. In MVA, the max/intermediate eigenvalue ratio is an indication of the accuracy of the coordinate definition. These FRs display a wide range in core field intensity (5-110 nT), and location in latitude (-75° - +75°) and longitude (1° - 358°). Of the 156 FRs selected, 140 contain sufficient electron data from SWEA to estimate magnetic topology. Below 160 km altitude, the superthermal electrons are dominated by local processes such as production and collisions which makes the topology score unreliable (*Xu et al.,* 2019). We therefore omit FR events that were detected below 160 km, leaving us with 121 events. The FRs that comprise our database exhibit three primary magnetic topologies (draped, open-dayside, closed-dayside). This variety in magnetic topology suggests that these FRs may have been formed via different formation mechanisms.

In order to categorize the formation mechanism of each FR, we examine the MAG, SWEA, and STATIC data for each event. An FR is assigned a formation mechanism of BWI, ER, or IR based on the following observations: if an FR were to form via the BWI mechanism, it would be populated primarily by solar wind electrons gyrating around magnetic field lines connected on both ends to the IMF and classified as a draped magnetic field line. Draped topology throughout an FR suggests that it had been formed via the BWI mechanism. If an FR formed via the ER mechanism, the “opening up” of crustal magnetic field lines would allow solar wind plasma to mix with the ionospheric plasma that previously populated the closed magnetic loops of the crustal anomalies. FRs formed via the ER mechanism would contain both solar wind electrons and photoelectrons and exhibit some open-dayside magnetic field topology. An FR formed via the IR mechanism would be surrounded by closed magnetic topology and contain exclusively photoelectrons because the FR does not require reconnection involving the IMF. FRs that exhibit closed-dayside magnetic topology throughout their structure are consistent with having been formed via the IR mechanism.

3.1 Case Studies

Figure **2** shows a time series of an FR signature in the MAVEN data. The FR can be identified by a characteristic increase in total magnetic field amplitude (Figure **2b**), and a unimodal peak in B_M coinciding with the inflection point of a bipolar signature in B_L (Figure **2c**). The shape parameter is >1 in both the away and towards directions throughout the FR signature (Figure **2e**), indicating that the FR is populated primarily by solar wind electrons rather than photoelectrons in both directions. Therefore, the topology score throughout the FR is 7 (Figure **2f**), indicating draped magnetic topology. Draped topology is expected if the FR were formed via the BWI mechanism illustrated in Figure **1a**. Of the 121 FRs in our database, 11 (9%) are consistent with

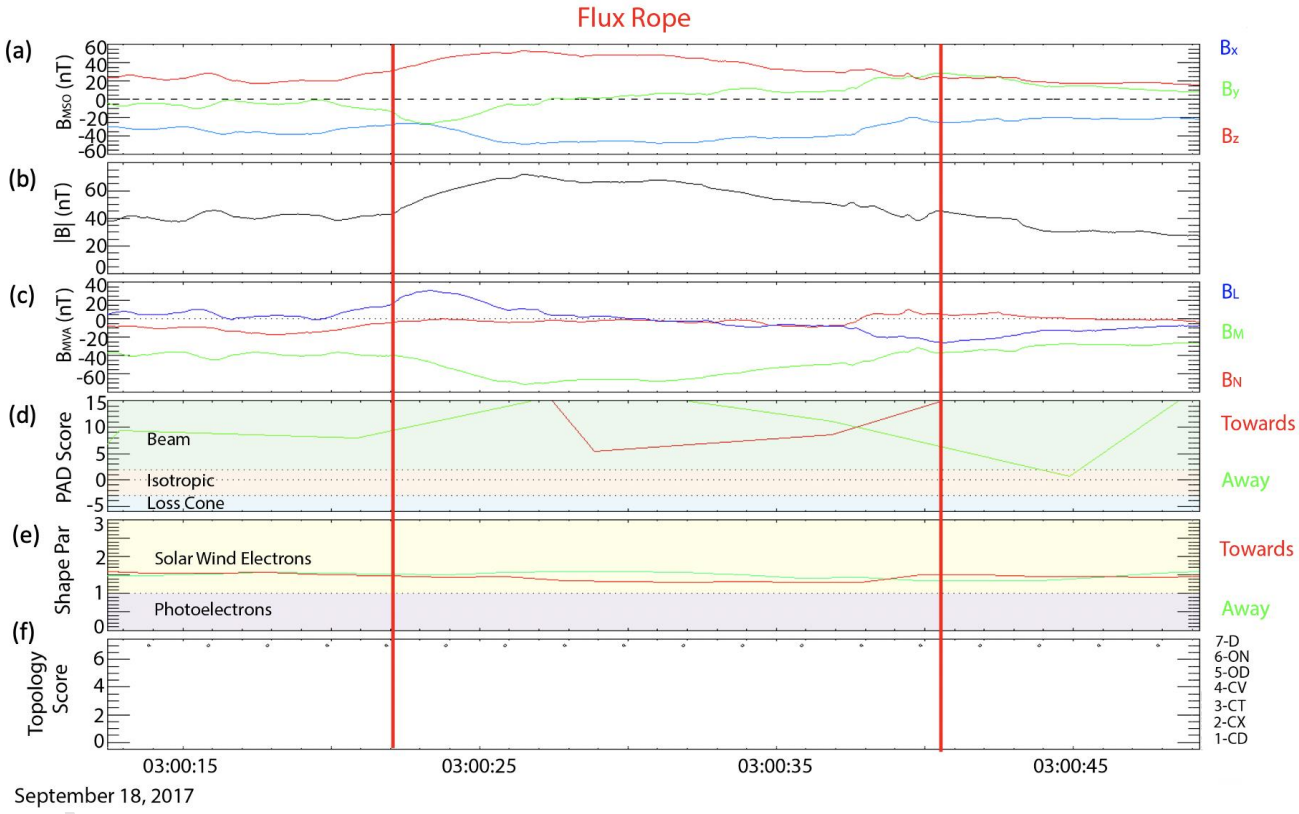

Figure **2**: *MAVEN observations of a flux rope detected on September 18, 2017, a) magnetic field in the MSO frame, b) magnetic field magnitude, c) magnetic field in MVA coordinate frame, d) PAD score, e) shape parameter, f) topology score*

having been formed via the BWI formation mechanism.

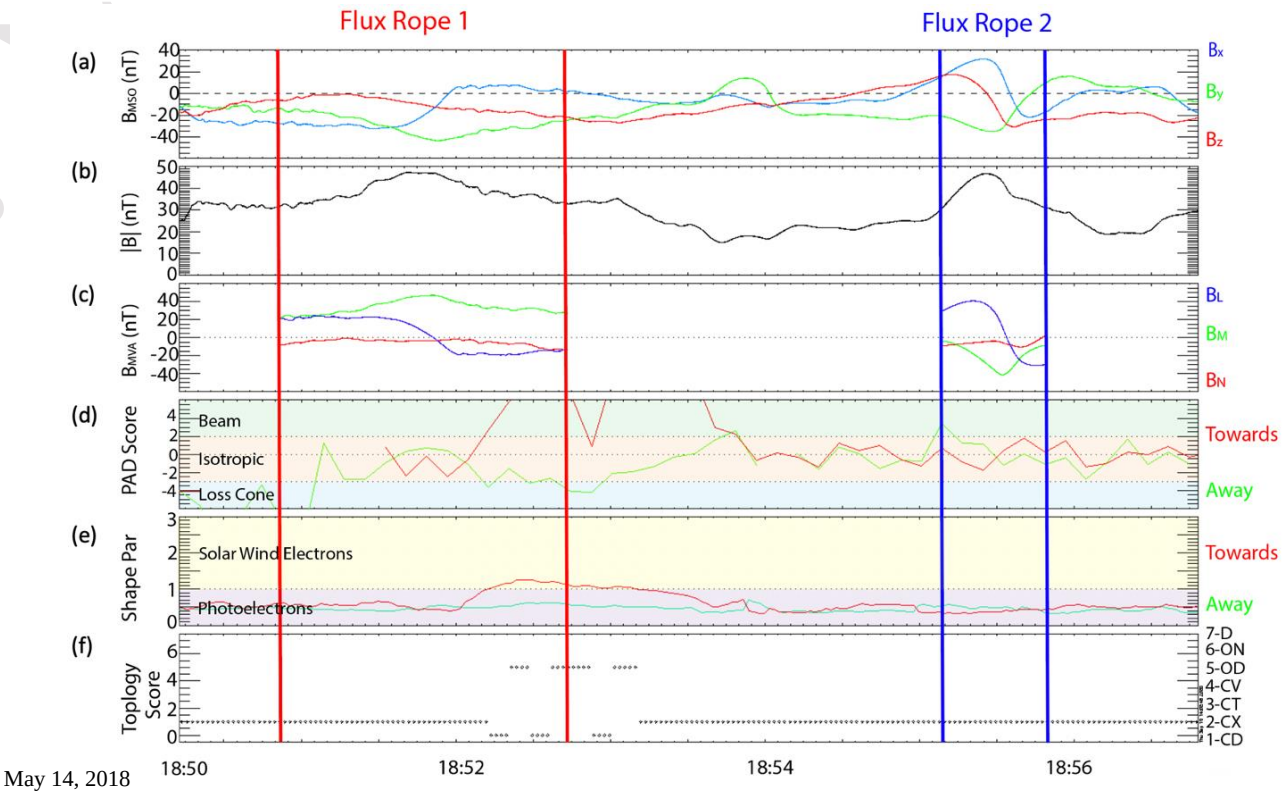

Figure **3**: MAVEN observations on May 14, 2018 in the same format as Figure **1**.

Figure **3** shows a time series of a pair of FRs detected by MAVEN on May 14, 2018. From the onset of the first FR to ~18:52:30 the shape parameter is < 1 (Figure **3e**) and the topology score = 1 (Figure **3f**), indicating the presence of photoelectrons and closed-dayside magnetic topology. For the remainder of the FR, the shape parameter in the towards direction remains >1, and the topology score = 5, indicating the presence of solar wind electrons and open-dayside magnetic topology. If an FR were to have been formed via the ER mechanism illustrated in Figure **1b**, we would expect at least part of the structure to exhibit open-dayside magnetic topology. 41 (34%) FRs in our database are consistent with having been formed via the ER formation mechanism.

The second FR shown in Figure **3** maintains a shape parameter <1 and a topology score of 1 throughout the structure, indicating the presence of photoelectrons and closed-dayside magnetic topology, respectively. Closed-dayside topology is expected if the FR were formed via the IR mechanism illustrated in Figure **1c**. 69 (57%) of the FRs in our database are consistent with having been formed via the IR formation mechanism.

4 Discussion

Figure **4a** shows histograms of altitudes at which FRs were detected, separated by formation mechanism and grouped within the same bins. BWI FRs tend to occur at higher altitudes (median altitude = 670 km) than ER or IR FRs (median altitudes = 222 and 198 km, respectfully), which is consistent with the idea that BWI FRs form closer to the boundary between the magnetosheath and ionospheric plasma. Furthermore, Figure **4b** shows the occurrence rate of FRs measured by MAVEN in different latitude bins. BWI FRs tend to occur more frequently near the poles. This is consistent with BWI FRs forming as a result of velocity shear because we expect the gradient

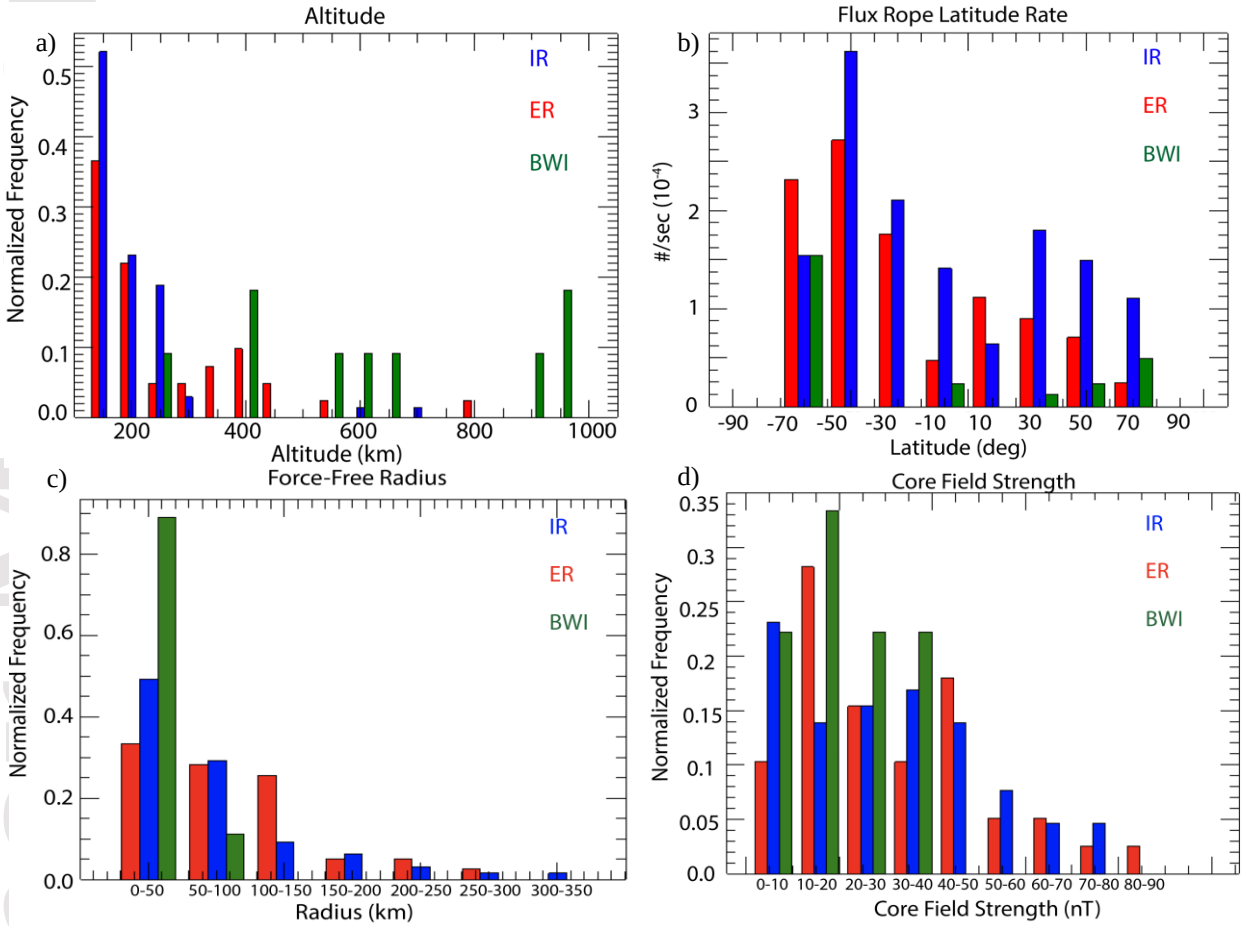

Figure **4**: *Flux rope properties separated by formation mechanism: a), Altitude at which the flux ropes were detected (km), b) flux rope occurrence rate at different latitudes (flux ropes/ second), c) flux rope radius estimated by the force-free model fit (km), d) Maximum field strength of the core field estimated by the force-free model (nT). Histograms of different formation mechanisms within the same bin on the horizontal axis are plotted side-by-side.*

between magnetosheath and ionospheric plasma to be greatest near the terminators. The ER and IR FRs occur most frequently in the mid-southern latitudes where the crustal magnetic fields are strongest, which is consistent with the notion that they were formed via reconnection between an anomaly and the IMF (ER), or reconnection of the crustal anomalies themselves (IR).

We implement a model in which FRs are assumed to be force-free ($\vec{\boldsymbol{J}} \times \vec{\boldsymbol{B}} = \mathbf{0}$) and stationary in order to estimate properties of the FRs including radii and core-field strength at the center of the structure. Assuming cylindrical symmetry, *Lepping et al.*, [1996] showed that the axial and tangential magnetic field of an FR can be expressed with Bessel functions:

$$\boldsymbol{B_A} = \boldsymbol{J_0}(\boldsymbol{\alpha r'})\boldsymbol{B_0}, \qquad \boldsymbol{B_T} = \boldsymbol{J_1}(\boldsymbol{\alpha r'})\boldsymbol{B_0 H}\,, \qquad \boldsymbol{B_r} = \mathbf{0}$$

$\boldsymbol{B_A}, \boldsymbol{B_T}, \boldsymbol{B_R}$ are the axial, tangential, and radial magnetic fields, $\boldsymbol{J_0}(\boldsymbol{\alpha r'})$, $\boldsymbol{J_1}(\boldsymbol{\alpha r'})$ are the zeroth- and first-order Bessel functions, $\boldsymbol{B_0}$ is the magnetic field magnitude of the FR's core, and $\boldsymbol{H}$ is the handedness of the helicity. The parameter $\boldsymbol{\alpha}$ is a constant at 2.4048 and represents the x-intercept of the zeroth-order Bessel function. The components of this modeled field thus depend on $\boldsymbol{r'}$, which is the radial distance from the center of the FR. We can apply this fitting technique to all 121 events in this study and implement a $\boldsymbol{\chi^2}$ test to select a radius that produces a best fit for each FR event. This best fit radius also allows us to estimate the absolute core-field strength of each event. Selecting for events where $\boldsymbol{\chi^2 <. 02}$, we find that 102 of the 121 FRs can be considered force-free. Of these 102 FRs, we see a variety of radius estimates (2 km – 311 km) and core-field strength (6-110 nT).

We produce a histogram of radius and core-field strength separated by estimated FR formation mechanism (Figure **4c**, **4d**). FRs formed through ER, IR have median radii of 64, 50 km, respectively. FRs formed through BWI are the smallest of the three, with a median radius of 5 km. This radius is in agreement with FRs found at Venus which have an estimated radius of ~10 km (*Luhmann et al.*,1985), further suggesting that these FRs may have formed via a process similar to that at unmagnetized objects like Venus and Titan. A previous statistical study of FR properties throughout the dayside and nightside of the Martian ionosphere (*Briggs et al.*, 2011) reported a median radius of 80 km ($\boldsymbol{\sigma}$=97 km) which is in agreement with the overall force-free FR radii in our study. This suggests the FRs analyzed in *Briggs et al.*, [2011] were likely formed by a variety of mechanisms including, but not limited to, ER and IR. Using data from the STATIC instrument, we are able to estimate the local gyroradius for three main species in the Martian ionosphere: H^+, O^+, and O_2^+ (median local gyroradii of 11 km, 74 km, and 113 km, respectively). If the radius of an FR is smaller than the gyroradius of a particle, then the particle cannot be frozen into the magnetic field of the FR, and the FR could not be a mechanism for ionospheric escape at Mars. Of the 102 FRs that are considered force-free, 77 (75%), 50(47%),

and 41 (40%) have radii larger than the local gyroradius of H^+, O^+, and O_2^+ , respectively. This suggests that only a fraction of the FRs found in our database may contribute to the escape of planetary ions. While BWI FRs are magnetically disconnected from the ionosphere and cannot play a role in ionospheric transport, there is no significant difference between the IR and ER FRs in their ability to lead to ionospheric escape via plasma entrainment and propagation downstream. The core-field strength of the BWI, ER, and IR FRs does not vary greatly depending on formation mechanism (median values of 25 nT, 33 nT, 33 nT, respectively). We note that there is a possibility of misclassification of FRs. If an FR were to form via multiple x-line external reconnection between an open magnetic field line and a draped IMF field line, it would produce an FR with both ends attached to the IMF, a draped topology score, and a classification of BWI. The disparity between FR sizes of BWI and ER FRs suggests that either the misclassification of FRs is uncommon, or that FRs formed via this mechanism are quite small and do not contribute to atmospheric mass loss.

5 Summary

We visually inspected over 1900 orbits in which MAVEN sampled the dayside ionosphere of Mars. We transformed the MAG data into MVA coordinates to identify 156 magnetic FRs within the Martian ionosphere. Electron data from the SWEA instrument were used to determine magnetic topology of the FRs in order to estimate their formation mechanism. Each of the three magnetic topologies (draped, open-dayside, closed-dayside) that comprise the FRs within our database are consistent with a distinct formation mechanism: 1) boundary wave instabilities (BWI) like KH similar to FRs observed at Venus 2) external reconnection (ER) between the IMF and the crustal anomalies 3) internal reconnection (IR) of the crustal anomalies themselves. The BWI FRs are the least common in our dataset, making up only 9% of the FRs, while the ER and the IR formation mechanisms make up 33% and 58% of the FRs, respectively. Using a force-free model fit, we were able to estimate the radii and core-field strength of 102 FRs. The radii of FRs range from 2 km-360 km, and the core-field strength range from 5 nT-110 nT. Interestingly, the properties of BWI FRs including altitude at which they are detected, latitude, and median radius differ from the ER and IR FRs. Comparisons between the local gyroradii of planetary ions and the radii of the FRs suggests that roughly a third of the ER and IR FRs are large enough to trap heavy ions like O^+ and O_2^+, while no BWI FRs could contribute to mass loss of planetary ions.

Acknowledgments, Samples, and Data

The MAVEN project is supported by NASA through the Mars Exploration Program. In accordance with the AGU data policy, MAVEN data are publicly available through the Planetary Plasma Interactions Node of the Planetary Data System (**https://pds-ppi.igpp.ucla.edu/mission/MAVEN**).

References

Acuña, M. H., et al. (1999), Global distribution of crustal magnetization discovered by the mars global surveyor MAG/ER experiment, Science, 284(5415), 790-793.

Beharrell, M., and J. Wild (2012), Stationary flux ropes at the southern terminator of Mars, Journal of Geophysical Research-Space Physics, 117(A12).

Brain, D., A. Baker, J. Briggs, J. Eastwood, J. Halekas, and T. Phan (2010), Episodic detachment of Martian crustal magnetic fields leading to bulk atmospheric plasma escape, Geophysical Research Letters, 37.

Briggs, J., D. Brain, M. Cartwright, J. Eastwood, and J. Halekas (2011), A statistical study of flux ropes in the Martian magnetosphere, Planetary and Space Science, 59(13), 1498-1505.

Cloutier, P., et al. (1999), Venus-like interaction of the solar wind with Mars, Geophysical Research Letters, 26(17), 2685-2688.

Connerney, J., J. Espley, P. Lawton, S. Murphy, J. Odom, R. Oliversen, and D. Sheppard (2015), The MAVEN Magnetic Field Investigation, Space Science Reviews, 195(1-4), 257-291.

DiBraccio, G., et al. (2015), MESSENGER observations of flux ropes in Mercury's magnetotail, Planetary and Space Science, 115, 77-89.

Elphic, R., C. Cattell, K. Takahashi, S. Bame, and C. Russell (1986), ISEE-1 and ISEE-2 Observations of Magnetic-Flux Ropes in the Magnetotail - FTES in the Plasma Sheet, Geophysical Research Letters, 13(7), 648-651.

Filippov, B., O. Martsenyuk, A. Srivastava, and W. Uddin (2015), Solar Magnetic Flux Ropes, Journal of Astrophysics and Astronomy, 36(1), 157-184.

Fu, Z., and L. Lee (1985), Simulation of Multiple X-Line Reconnection at the Dayside Magnetopause, Geophysical Research Letters, 12(5), 291-294.

Hara, T., K. Seki, H. Hasegawa, D. Brain, K. Matsunaga, M. Saito, and D. Shiota (2014), Formation processes of flux ropes downstream from Martian crustal magnetic fields inferred from Grad-Shafranov reconstruction, Journal of Geophysical Research-Space Physics, 119(9), 7947–7962.

Hara, T., et al. (2017), MAVEN observations of a giant ionospheric flux rope near Mars resulting from interaction between the crustal and interplanetary draped magnetic fields, Journal of Geophysical Research-Space Physics, 122(1), 828-842.

Jakosky, B. M., M. Slipski, M. Benna, P. Mahaffy, M. Elrod, R. Yelle, S. Stone, and N. Alsaeed (2017), Mars' atmospheric history derived from upper-atmosphere measurements of, Science, 355(6332), 1408-1410.

Jasinski, J., J. Slavin, C. Arridge, G. Poh, X. Jia, N. Sergis, A. Coates, G. Jones, and J. Waite (2016), Flux transfer event observation at Saturn's dayside magnetopause by the Cassini spacecraft, Geophysical Research Letters, 43(13), 6713-6723.

Lepping, R., J. Slavin, M. Hesse, J. Jones, and A. Szabo (1996), Analysis of magnetotail flux ropes with strong core fields: ISEE 3 observations, Journal of Geomagnetism and Geoelectricity, 48(5-6), 589-601.

Luhmann, J., and R. Elphic (1985), On the Dynamo Generation of Flux Ropes in the Venus Ionosphere, Journal of Geophysical Research-Space Physics, 90(NA12), 2047-2056.

Martin, C., C. Arridge, S. Badman, C. Russell, and H. Wei (2020), Distribution and Properties of Magnetic Flux Ropes in Titan's Ionosphere, Journal of Geophysical Research-Space Physics, 125(4), 1029-1043.

McFadden, J., et al. (2015), MAVEN SupraThermal and Thermal Ion Compostion (STATIC) Instrument, Space Science Reviews, 195(1-4), 199-256.

Mitchell, D., et al. (2016), The MAVEN Solar Wind Electron Analyzer, Space Science Reviews, 200(1-4), 495-528.

Morgan, D., D. Gurnett, F. Akalin, D. Brain, J. Leisner, F. Duru, R. Frahm, and J. Winningham (2011), Dual-spacecraft observation of large-scale magnetic flux ropes in the Martian ionosphere, Journal of Geophysical Research-Space Physics, 116.

Möstl, U., N. Erkaev, M. Zellinger, H. Lammer, H. Groller, H. Biernat, and D. Korovinskiy (2011), The Kelvin-Helmholtz instability at Venus: What is the unstable boundary?, Icarus, 216(2), 476-484.

Penz, T., et al. (2004), Ion loss on Mars caused by the Kelvin-Helmholtz instability, Planetary and Space Science, 52(13), 1157-1167.

Ruhunusiri, S., et al. (2016), MAVEN observations of partially developed Kelvin-Helmholtz vortices at Mars, Geophysical Research Letters, 43(10), 4763-4773.Russell, C. (1990), Magnetic Flux Ropes in the Ionosphere of Venus, Physics of Magnetic Flux Ropes, edited, pp. 413-423, Geophysical Monograph, American Geophysical Union, Washington, DC.

Slavin, J., R. Lepping, J. Gjerloev, D. Fairfield, M. Hesse, C. Owen, M. Moldwin, T. Nagai, A. Ieda, and T. Mukai (2003), Geotail observations of magnetic flux ropes in the plasma sheet, Journal of Geophysical Research-Space Physics, 108(A1), 1015-1033.

Soobiah, Y., J. Wild, M. Beharrell, S. Barabash, R. Lillis, D. Mitchell, A. Coates, J. Winningham, and R. Frahm (2014), Properties of a large-scale flux rope and current sheet region on the dayside of Mars: MGS MAG/ER and MEX ASPERA-3 ELS observations, Icarus, 242, 297-315.

Sonnerup, B. U. Ö., and M. Scheible (1998), Minimum and maximum variance analysis, in Analysis Methods for Multi-Spacecraft Data, ISSI Sci. Rep. no. SR-001, edited by G. Paschmann and P. W. Daly, chap. 8, pp. 185–220, European Space Agency, Noordwijk, Netherlands.

Sun, W., S. Fu, J. Slavin, J. Raines, Q. Zong, G. Poh, and T. Zurbuchen (2016), Spatial distribution of Mercury's flux ropes and reconnection fronts: MESSENGER observations, Journal of Geophysical Research-Space Physics, 121(8), 7590-7607.

Terada, N., S. Machida, and H. Shinagawa (2002), Global hybrid simulation of the Kelvin-Helmholtz instability at the Venus ionopause, Journal of Geophysical Research-Space Physics, 107(A12), 1471.

Vignes, D., M. Acuna, J. Connerney, D. Crider, H. Reme, and C. Mazelle (2004), Magnetic flux ropes in the Martian atmosphere: Global characteristics, Space Science Reviews, 111(1-2), 223-231.

Weber, T., D. Brain, D. Mitchell, S. Xu, J. Connerney, and J. Halekas (2017), Characterization of Low-Altitude Nightside Martian Magnetic Topology Using Electron Pitch Angle Distributions, Journal of Geophysical Research-Space Physics, 122(10), 9777-9789.

Wei, H., C. Russell, T. Zhang, and M. Dougherty (2010), Comparison study of magnetic flux ropes in the ionospheres of Venus, Mars and Titan, Icarus, 206(1), 174-181.

Wolff, R. S., B. E. Goldstein, and C. M. Yeates (1980), The onset and development of Kelvin-Helmholtz instabilities at the Venus ionopause, Journal of Geophysical Research: Space Physics, 85(A13), , 7697–7707.

Xu, S., T. Weber, D. Mitchell, D. Brain, C. Mazelle, G. DiBraccio, and J. Espley (2019), A Technique to Infer Magnetic Topology at Mars and Its Application to the Terminator Region, Journal of Geophysical Research-Space Physics, 124(3), 1823-1842.

Xu, S., et al. (2017), Martian low-altitude magnetic topology deduced from MAVEN/SWEA observations, Journal of Geophysical Research-Space Physics, 122(2), 1831-1852.

Figure 1.

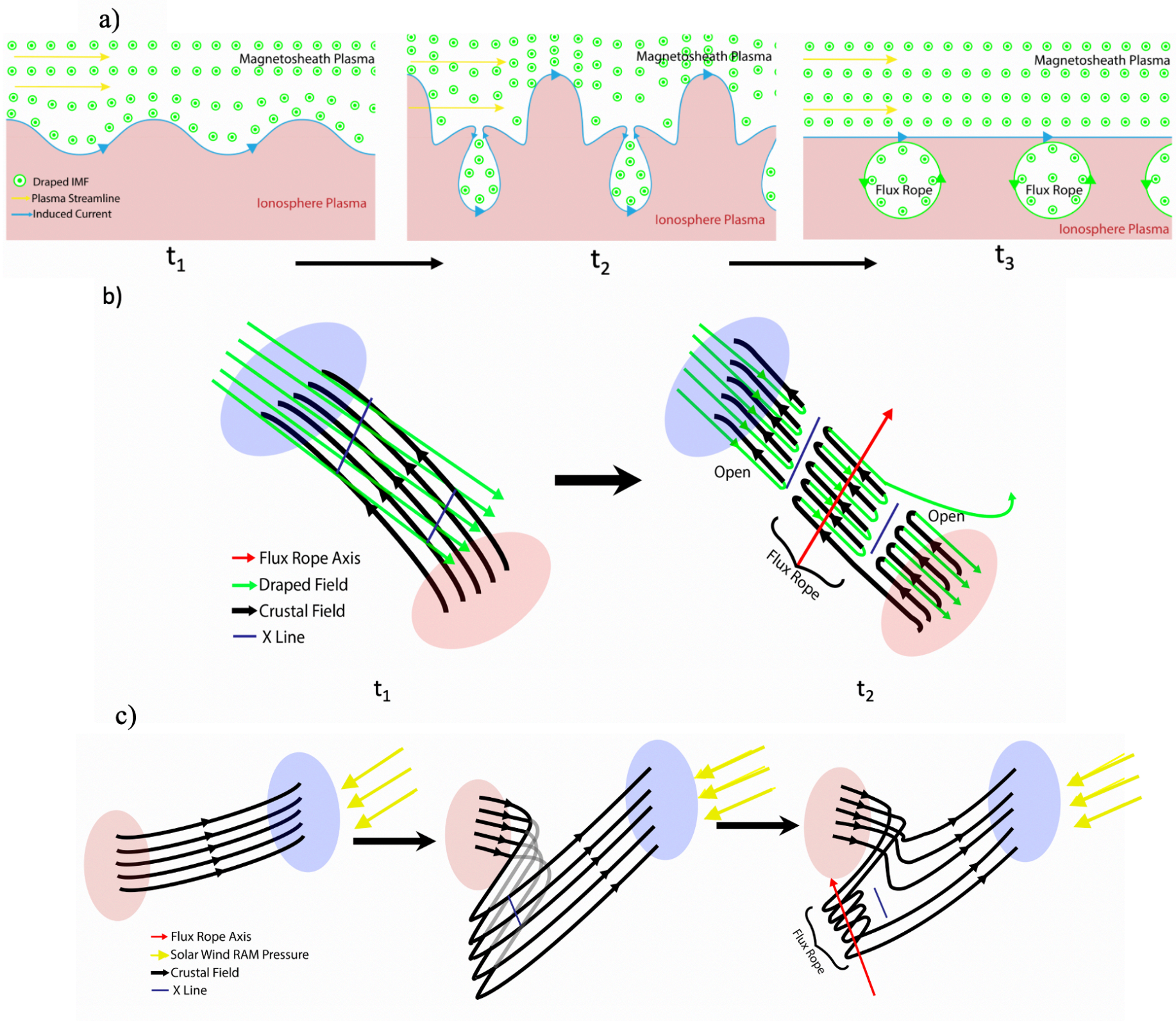
a)
Magnetosheath Plasma
Draped IMF
Plasma Streamline
Induced Current
Ionosphere Plasma
Magnetosheath Plasma
Ionosphere Plasma
Magnetosheath Plasma
Flux Rope
Flux Rope
Ionosphere Plasma
t1
t2
t3
b)
Flux Rope Axis
Draped Field
Crustal Field
X Line
Open
Open
Flux Rope
t1
t2
c)
Flux Rope Axis
Solar Wind RAM Pressure
Crustal Field
X Line
Flux Rope

Figure 2.

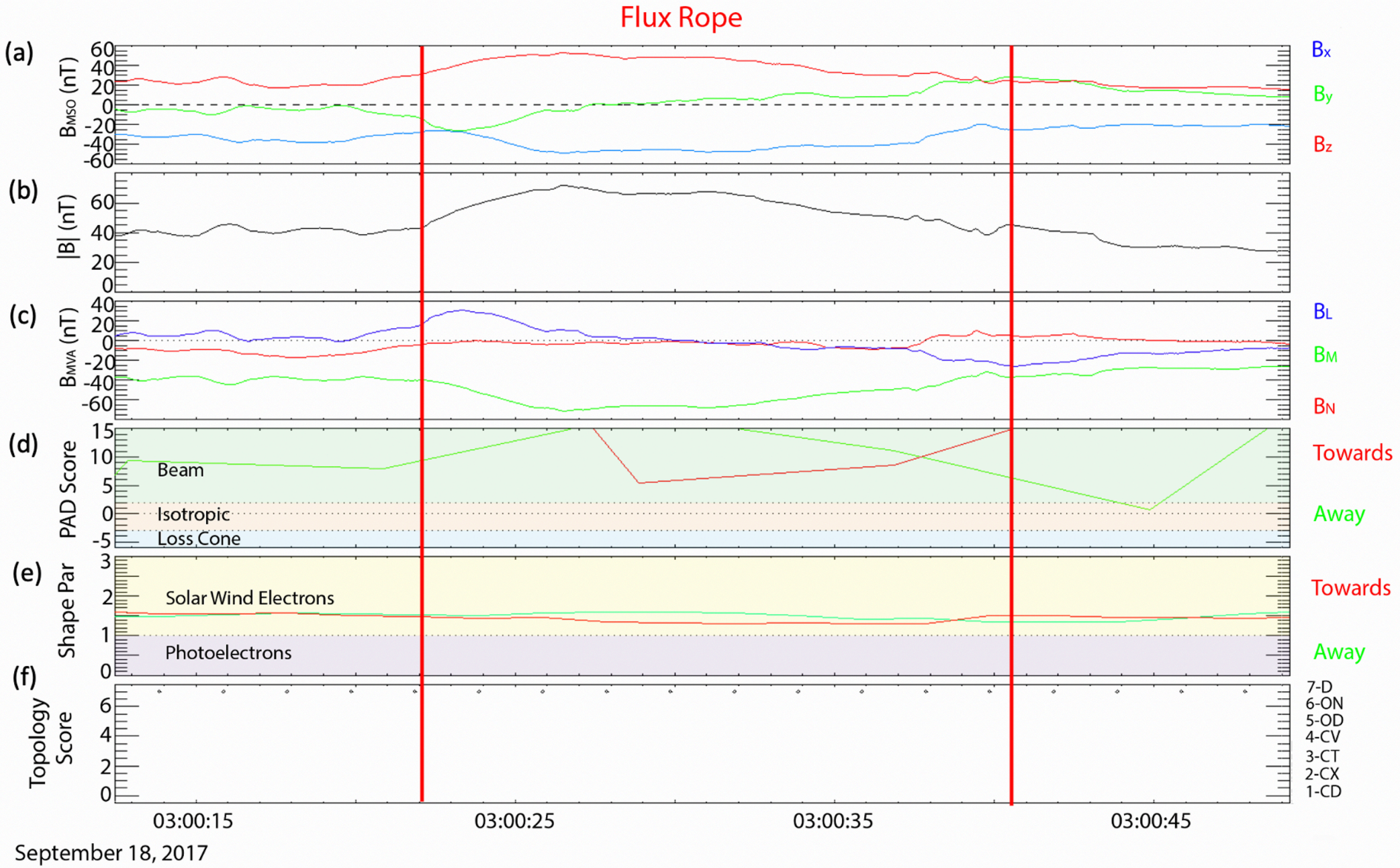

Figure 3.

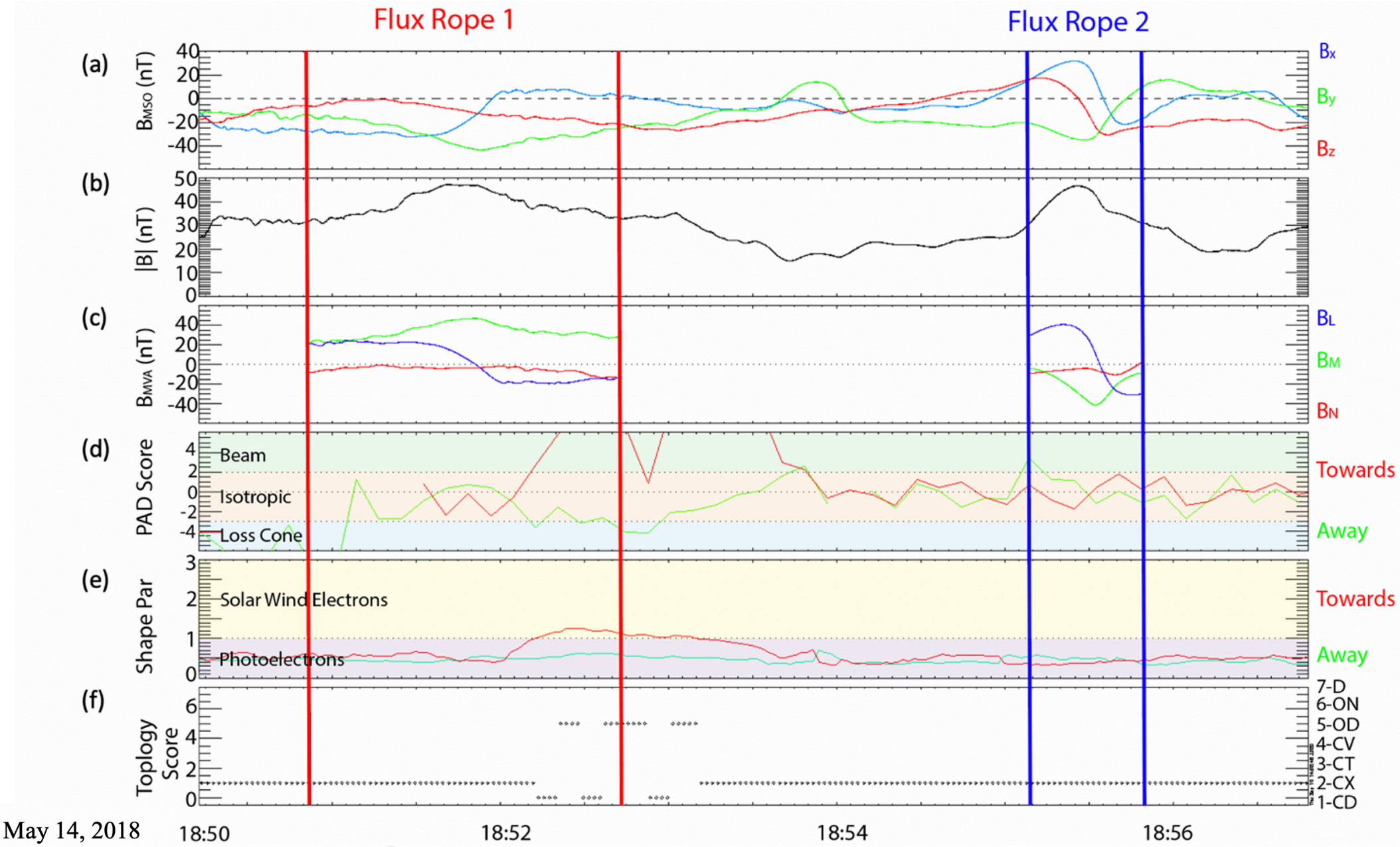

Figure 4.

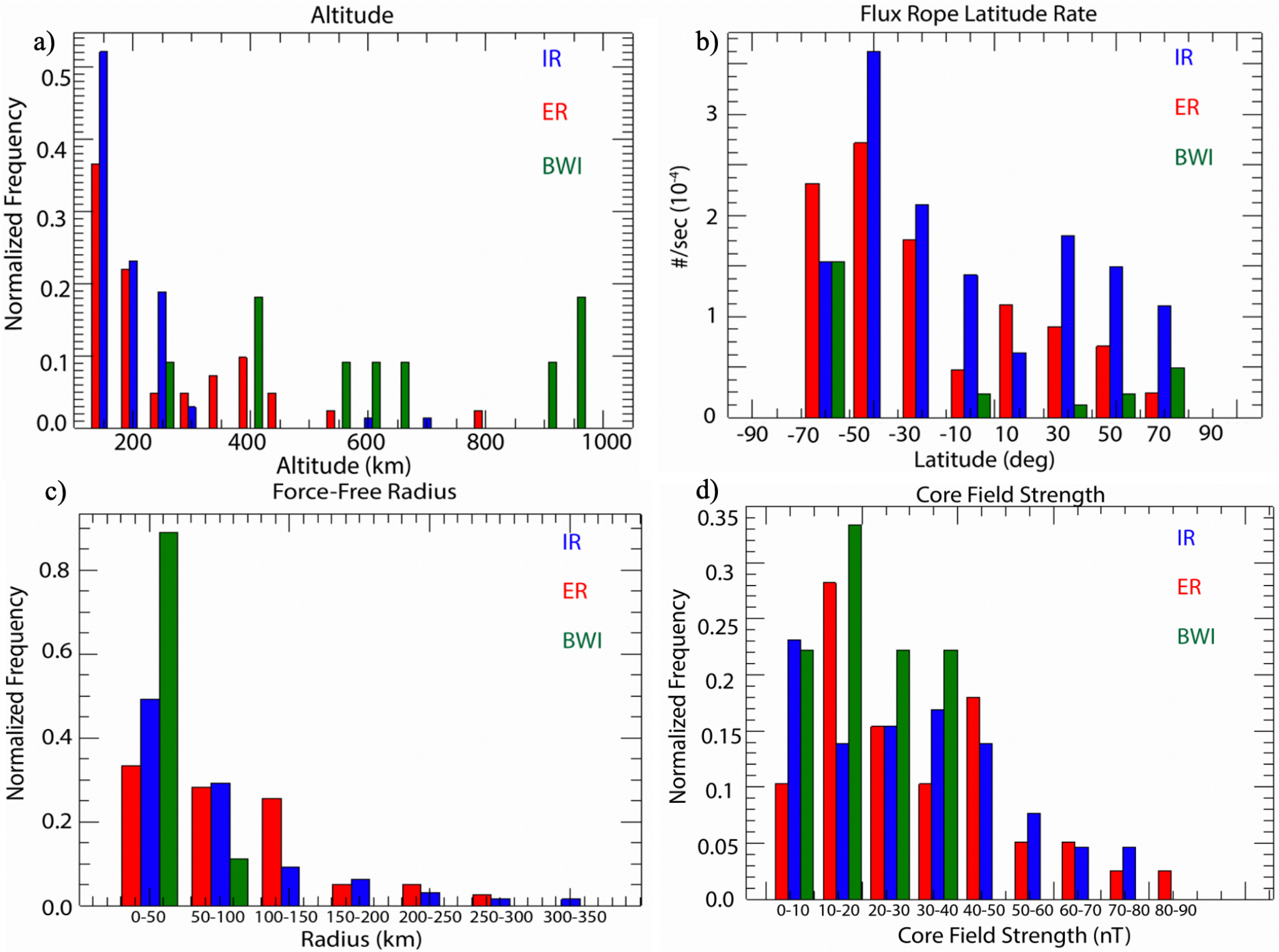
a)
Altitude
Normalized Frequency
0.0
0.1
0.2
0.3
0.4
0.5
200
400
600
800
1000
Altitude (km)
IR
ER
BWI
b)
Flux Rope Latitude Rate
#/sec (10⁻⁴)
0
1
2
3
-90
-70
-50
-30
-10
10
30
50
70
90
Latitude (deg)
IR
ER
BWI
c)
Force-Free Radius
Normalized Frequency
0.0
0.2
0.4
0.6
0.8
0-50
50-100
100-150
150-200
200-250
250-300
300-350
Radius (km)
IR
ER
BWI
d)
Core Field Strength
Normalized Frequency
0.0
0.05
0.1
0.15
0.2
0.25
0.3
0.35
0-10
10-20
20-30
30-40
40-50
50-60
60-70
70-80
80-90
Core Field Strength (nT)
IR
ER
BWI